INTERNATIONAL JOURNAL FOR NUMERICAL METHODS IN FLUIDS, VOL. 7, 621–633 (1987)

APPLICATION OF AN EXPLICIT TVD SCHEME FOR UNSTEADY, AXISYMMETRIC, MUZZLE BRAKE FLOW

C. H. COOKE*

Old Dominion University, Department of Mathematics, Norfolk, VA 23508, U.S.A.

SUMMARY

Operator splitting in the presence of source terms is necessary in order to apply Harten's second-order accurate, total-variation-diminishing (TVD), shock-capturing scheme to higher-dimensional problems. By employing Godunov boundary treatment at the muzzle brake, such splitting is applied to the problem of muzzle brake flow simulation for the case of blasts which are impeded, by vertical and slanted baffles, respectively. Results from numerical studies of various types of wall boundary condition treatment which are consistent with Harten's TVD scheme are indicated.

KEY WORDS TVD Schemes Shock Capturing Muzzle Brake Flow Blast Wave Simulation Harten's Method Operator Splitting

INTRODUCTION

Rapid discharge of a propellant gas from the muzzle blast of a weapon induces the formation of a strong shock wave which propagates into the environment. The ensuing flow is characterized by formation of secondary shocks and contact surfaces within the developing plume. Following Godunov's classical development of the first widely effective first-order accurate shock-capturing scheme,[1] Sod[2] gives a survey of several early finite difference schemes for calculation of shocked flow. State of the art, second-order accurate, shock capturing techniques for numerical calculation of such flows have been constructed in recent years by Van Leer,[3] Colella and Woodward,[4] Harten,[5] Roe[6] and Osher.[7] The object of the present report is to consider some problems which arise in applying Harten's method to the numerical solution of muzzle blast problems governed by the Euler equations in axisymmetric co-ordinate systems.

For the case of a vertical muzzle brake, Harten's method can be applied through the use of operator splitting, as advocated by Strang.[8] Methods for splitting in the presence of source terms have further been investigated by the author.[9] However, the case of a slanted muzzle brake requires modification of the method. The use of an orthogonal curvilinear co-ordinate transformation has been recommended by Yee.[10] Our solution to this problem, which avoids curvilinear transformations, is to develop a hybrid scheme. Here Godunov's method[1] is used near the brake, whereas Harten's method is applied on a uniform grid away from the vicinity of the brake. For weak blasts this method appears workable. In any case, the problems arising from this approach are

---

*This research was performed, in part, at the U.S. Army Ballistic Research Laboratory, Aberdeen Proving Ground, Aberdeen, Maryland, U.S.A., Spring, 1985. Conclusions given are personal, and do not necessarily reflect opinions of the U.S. Army.

0271–2091/87/060621–13$06.50

Received 19 November 1985
Revised 10 October 1986

probably no worse than the difficulty of applying boundary conditions at the slanted baffle when using curvilinear transformations.

THE EULER EQUATIONS

The Euler equations of gas dynamics can be written in strong conservation form as

$$\frac{\partial \mathbf{Q}}{\partial t}+\frac{\partial \mathbf{F}(\mathbf{Q})}{\partial x}+\frac{\partial \mathbf{G}(\mathbf{Q})}{\partial y}+\mathbf{W}(\mathbf{Q})=\mathbf{0}, \tag{1a}$$

where

$$\mathbf{Q}=\begin{bmatrix}\rho\\ m\\ n\\ e\end{bmatrix},\quad \mathbf{F}=\begin{bmatrix}m\\ \frac{m^2}{\rho}+p\\ mv\\ (e+p)\frac{m}{\rho}\end{bmatrix},\quad \mathbf{G}=\begin{bmatrix}n\\ nu\\ \frac{n^2}{\rho}+p\\ (e+p)\frac{n}{\rho}\end{bmatrix}, \tag{1b}$$

$$\mathbf{W}=\frac{\varepsilon n}{y}\begin{bmatrix}1\\ \frac{m}{\rho}\\ \\ \frac{n}{\rho}\\ E+p/\rho\end{bmatrix}, \tag{1c}$$

where the respective choices $\varepsilon=0$ or 1 allow either a Cartesian or an axisymmetric co-ordinate system. In these equations, ρ is the density; $m=\rho u$, $n=\rho v$ are the components of momentum and u, v are velocities in the x- and y-directions, respectively; p is the pressure; E is the specific total energy, related to the specific internal energy, $\bar{e}$ by

$$E=\bar{e}+\frac{u^2+v^2}{2};\quad e=\rho E; \tag{2}$$

and the equation of state is

$$p=(\gamma-1)\rho\bar{e}, \tag{3}$$

where γ is the ratio of specific heats.

EIGENVECTOR PROJECTION

The second-order accurate, total-variation-diminishing scheme of Harten is well-documented.[5,10,11] As this scheme in its original conception is applicable only to the Euler equations in one space dimension, operator splitting of equation (1) into three separate components will be employed. To avoid repetition, the equations for the x- and y-sweeps can both be accommodated by the following device: consider application of Harten's method to an equation

$$\frac{\partial \mathbf{Q}}{\partial t}+\frac{\partial \hat{\mathbf{F}}}{\partial \varepsilon}(\mathbf{Q})=\mathbf{0}, \tag{4}$$

where $\mathbf{F}(\mathbf{Q})$ has the Jacobian matrix

$$\mathbf{A} = \xi_x \mathbf{A} + \xi_y \mathbf{B}, \tag{5}$$

with $\mathbf{A} = \partial \mathbf{F}/\partial \mathbf{Q}$ and $\mathbf{B} = \partial \mathbf{G}/\partial \mathbf{Q}$. Then, respective choices of $\xi = x$ or $\xi = y$ (in equations (4) and (5), and in the development below) yield Cartesian x- and y- splittings for equation (1). Carofano[11] advocates incorporation of the source term through the third (split) equation

$$\frac{\partial \mathbf{Q}}{\partial t} + \mathbf{W}(\mathbf{Q}) = \mathbf{0}. \tag{6}$$

By using the device (4), (5), a single subroutine for applying Harten's scheme on both the x- and y-sweeps can be developed, by simply inputting $\xi_x = 1$, $\xi_y = 0$ or vice versa, as the sweep requires.

Let c be the local speed of sound; the eigenvalues of $\hat{\mathbf{A}}$ are[12]

$$(a^1, a^2, a^3, a^4) = (\hat{U} - c, \hat{U}, \hat{U} + c, \hat{U}), \tag{7}$$

where

$$\hat{U} = \frac{\xi_x u + \xi_y v}{\sqrt{(\xi_x^2 + \xi_y^2)}} = k_1 u + k_2 v. \tag{8}$$

Furthermore, let $\mathbf{R} = (\mathbf{R}^1, \mathbf{R}^2, \mathbf{R}^3, \mathbf{R}^4)$ be the matrix whose columns are the eigenvectors of $\mathbf{A}$, where $\mathbf{R} = \mathbf{R}(\xi_x, \xi_y)$. A choice of $\mathbf{R}$ and $\mathbf{R}^{-1}$ can be written[10]

$$\mathbf{R} = \begin{bmatrix} 1 & 1 & 1 & 0 \\ u - k_1 c & u & u + k_1 c & k_2 \\ v - k_2 c & v & v + k_2 c & -k_1 \\ H - k_1 uc - k_2 vc & \dfrac{u^2 + v^2}{2} & H + k_1 uc + k_2 vc & k_2 u - k_1 v \end{bmatrix}, \tag{9}$$

where k_1 and k_2 are determined from equation (8) and

$$H = \frac{c^2}{\gamma - 1} + \frac{u^2 + v^2}{2}; \tag{10}$$

and

$$\mathbf{R}^{-1} = \begin{bmatrix} \frac{1}{2}(b_1 + k_1 u/c + k_2 v/c) & -\frac{1}{2}(b_2 u + k_1/c) & -\frac{1}{2}(b_2 v + k_2/c) & \frac{1}{2} b_2 \\ 1 - b_1 & b_2 u & b_2 v & -b_2 \\ \frac{1}{2}(b_1 - k_1 u/c - k_2 v/c) & -\frac{1}{2}(b_2 u - k_1/c) & -\frac{1}{2}(b_2 v - k_2/c) & \frac{1}{2} b_2 \\ -k_2 u + k_1 v & k_2 & -k_1 & 0 \end{bmatrix}, \tag{11a}$$

with

$$b_1 = b_2(u^2 + v^2)/2, \tag{11b}$$

$$b_2 = (\gamma - 1)/c^2. \tag{11c}$$

Let a uniform grid spacing $\Delta x, \Delta y$ be introduced, with

$$x_j = j \Delta x, \quad y_k = k \Delta y.$$

Denote by $\mathbf{Q}_{j+1/2,k}$ some symmetric average (the Roe average[13] was used for computational experiments) of $\mathbf{Q}_{j,k}$ and $\mathbf{Q}_{j+1,k}$. Let $a^l_{j+1/2}$, $\mathbf{R}_{j+1/2}$, $\mathbf{R}^{-1}_{j+1/2}$ denote evaluations of a^l, $\mathbf{R}$, $\mathbf{R}^{-1}$ on the symmetric average $\mathbf{Q}_{j+1/2,k}$. We define

$$\boldsymbol{\alpha}_{j+1/2} = \mathbf{R}^{-1}_{j+1/2}(\mathbf{Q}_{j+1,k} - \mathbf{Q}_{j,k}) \tag{12}$$

as the component of

$$\Delta_{j+1/2}\mathbf{Q} = \mathbf{Q}_{j+1,k} - \mathbf{Q}_{j,k} \tag{13}$$

in the lth characteristic ε-direction.[5] The vector $\boldsymbol{\alpha}$ of equation (12) can be written as

$$\begin{bmatrix} \alpha^1 \\ \alpha^2 \\ \alpha^3 \\ \alpha^4 \end{bmatrix}_{j+1/2} = \begin{bmatrix} \dfrac{\text{aa} - \text{bb}}{2} \\ \Delta_{j+1/2}\rho - \text{aa} \\ \dfrac{\text{aa} + \text{bb}}{2} \\ \text{cc} \end{bmatrix}, \tag{14a}$$

where

$$\text{aa} = \frac{\gamma - 1}{c^2_{j+1/2}}\left[\Delta_{j+1/2}e + \frac{u^2_{j+1/2} + v^2_{j+1/2}}{2}\Delta_{j+1/2}\rho - u_{j+1/2}\Delta_{j+1/2}m - v_{j+1/2}\Delta_{j+1/2}n\right], \tag{14b}$$

$$\text{bb} = \frac{1}{c_{j+1/2}}[k_1\Delta_{j+1/2}m - (k_1u_{j+1/2} + k_2v_{j+1/2})\Delta_{j+1/2}\rho + k_2\Delta_{j+1/2}n], \tag{14c}$$

$$\text{cc} = -k_1\Delta_{j+1/2}n - (k_2u_{j+1/2} - k_1v_{j+1/2})\Delta_{j+1/2}\rho + k_2\Delta_{j+1/2}m, \tag{14d}$$

with

$$\Delta_{j+1/2}\rho = \rho_{j+1,k} - \rho_{j,k}, \quad \Delta_{j+1/2}m = m_{j+1,k} - m_{j,k} \tag{14e}$$

and

$$\Delta_{j+1/2}n = n_{j+1,k} - n_{j,k}, \quad \Delta_{j+1/2}e = e_{j+1,k} - e_{j,k}. \tag{14f}$$

The simplest form for $\mathbf{Q}_{j+1/2,k}$ is

$$\mathbf{Q}_{j+1/2,k} = (\mathbf{Q}_{j+1,k} + \mathbf{Q}_{j,k})/2. \tag{15}$$

Roe's form of the averaging in the ξ-direction is

$$u_{j+1/2,k} = \frac{\bar{D}u_{j+1,k} + u_{j,k}}{\bar{D} + 1}, \tag{16a}$$

$$u_{j+1/2,k} = \frac{\bar{D}v_{j+1,k} + v_{j,k}}{\bar{D} + 1}, \tag{16b}$$

$$H_{j+1/2,k} = \frac{\bar{D}H_{j+1,k} + H_{j,k}}{\bar{D} + 1}, \tag{16c}$$

$$c^2_{j+1/2,k} = (\gamma - 1)[H_{j+1/2,k} - \tfrac{1}{2}(u^2_{j+1/2,k} + v^2_{j+1/2,k})], \tag{16d}$$

$$\bar{D} = \sqrt{(\sigma_{j+1,k}/\sigma_{j,k})}, \tag{16e}$$

$$H = \frac{\gamma p}{(\gamma - 1)\rho} + \frac{1}{2}(u^2 + v^2). \tag{16f}$$

Similarly, Roe's averaging can be obtained for $u_{j,k+1/2}$, $v_{j,k+1/2}$ and $c_{j,k+1/2}$. In the numerical experiments Roe's averaging is used, as this is thought to give better results than (15).

A TVD ALGORITHM

Assume that operator splitting is to be employed in solving equation (1) on a uniform grid. The flux terms are updated by applying Harten's method individually to equation (4), with $\xi = x$ and $\xi = y$,

respectively; Euler's predictor–corrector method is applied to update equation (6). The solution at time τ is advanced to time $t + 2\tau$ by application of the following sequence of operators:

$$\mathbf{Q}_{j,k}^{n+2} = L_x L_y L_s L_s L_y L_x \mathbf{Q}_{j,k}^{n}, \tag{17}$$

where

$$L_x: \mathbf{Q}_{j,k}^{*} = \mathbf{Q}_{j,k}^{n} - \frac{\Delta t}{\Delta x}(\hat{\mathbf{F}}_{j+1/2,k}^{n} - \hat{\mathbf{F}}_{j-1/2,k}^{n}), \tag{18a}$$

$$L_y: \mathbf{Q}_{j,k}^{**} = \mathbf{Q}_{j,k}^{*} - \frac{\Delta t}{\Delta y}(\hat{\mathbf{G}}_{j,k+1/2}^{n} - \hat{\mathbf{G}}_{j,k-1/2}^{n}), \tag{18b}$$

$$L_s: \bar{\mathbf{Q}}_{j,k} = \mathbf{Q}_{j,k}^{**} - \Delta t \mathbf{W}(\mathbf{Q}_{j,k}^{**}), \tag{18c}$$

$$\mathbf{Q}_{j,k}^{n+1} = [\mathbf{Q}_{j,k}^{**} + \bar{\mathbf{Q}}_{j,k} - \Delta t \mathbf{W}(\bar{\mathbf{Q}}_{j,k})]/2. \tag{18d}$$

The numerical flux $\hat{\mathbf{F}}_{j+1/2,k}$ is given by

$$\hat{\mathbf{F}}_{j+1/2,k} = \left[\mathbf{F}(\mathbf{Q}_{j,k}) + \mathbf{F}(\mathbf{Q}_{j+1,k}) + \frac{\Delta x}{\Delta t} \sum_{l=1}^{4} B_{j+1/2,k}^{l} \mathbf{R}_{j+1/2,k}^{l} \right] \Big/ 2, \tag{19a}$$

$$B_{j+1/2,k}^{l} = g_{j,k}^{l} + g_{j+1,k}^{l} - P(v_{j+1/2,k}^{l} + \gamma_{j+1/2,k}^{l}) \alpha_{j+1/2,k}^{l}, \tag{19b}$$

$$g_{j,k}^{l} = s_{j+1/2,k}^{l} \max [0, \min (\alpha_{j+1/2,k}^{l}, \alpha_{j-1/2,k}^{l} s_{j+1/2,k}^{l})]/8, \tag{19c}$$

$$s_{j+1/2,k}^{l} = \operatorname{sign}(\alpha_{j+1/2,k}^{l}), \tag{19d}$$

$$\gamma_{j+1/2,k}^{l} = \begin{cases} (g_{j+1,k}^{l} - g_{j,k}^{l})/\alpha_{j+1/2,k}^{l}, & \alpha_{j+1/2,k}^{l} \neq 0, \\ 0, & \alpha_{j+1/2,k}^{l} = 0, \end{cases} \tag{19e}$$

$$v_{j+1/2,k}^{l} = \frac{\Delta t}{\Delta x} a_{j+1/2,k}^{l}, \tag{19f}$$

$$P(z) = z^2 + \tfrac{1}{4}. \tag{19g}$$

The subscript $j + \frac{1}{2}$ denotes a quantity evaluated on the (Roe) average state, as discussed in the preceding section (see equations (12)–(16)). No artificial compression terms[5] have been included in the algorithm. Such terms can give non-physical results in regions of flow expansion, necessitating complicated program switching or interactive processing in order to anticipate such occurrences.

The equations for the numerical flux $\hat{\mathbf{G}}_{j,k+1/2}$ may be obtained from equations (19) by replacing $\mathbf{F}$ with $\mathbf{G}$, Δx with Δy and $(j + \frac{1}{2}, k)$ indices with $(j, k + \frac{1}{2})$ indices. When equation (18c) is applied at a point $y = 0$, if $\varepsilon \neq 0$ it becomes necessary to apply L'Hospital's rule in evaluating the source term, $\mathbf{W}$, as v, y approach zero.

BOUNDARY-CONDITION IMPLEMENTATION

Since Harten's second-order method is a five-point difference scheme, at boundary points two pieces of information are necessary, whereas only Dirichlet or Neumann data is all that is required for a mathematically well-posed problem. Thus, at a sonic inflow one may be tempted to hold the inflow values constant over two mesh columns. As this implies the vanishing of streamwise derivatives on the inflow, problems may arise; particularly if, in addition, flow around a corner is involved. However, for supersonic flow this corner problem may be somewhat alleviated, by employing the Prandtl–Meyer expansion and Mach waves off the corner to calculate a second column of values which realistically reflect streamwise conditions.

At a wall boundary, Yee, Warming and Harten[14] advocate methods for approximating a zero

normal derivative in pressure, second-order accurate, which in practice is certainly consistent with the Euler equations evaluated at the wall. Carofano[15] suggests reflection, imaging points P_1, P_2 with P_4, P_5; the wall being located at P_3 (of course, the normal velocity component is reflected with a change in sign). A more compact reflection, which we advocate, consists of locating the wall halfway between P_2 and P_3, with P_1, P_2 the reflection of P_3, P_4. Wall flux is now calculated using the method of Widhopf and Buell.[16] This approach avoids consideration of what to do at corner points, as now there are no cell centres on the wall.

At outflow boundaries, which are usually located as far as possible from regions of interest, non-reflecting boundary conditions are usually employed. These can consist of extrapolation techniques, from interior to the boundary; or others, such as exhausting the outflow to cells having semi-infinite volumes.[16]

NUMERICAL RESULTS: VERTICAL BAFFLE

Gion and Schmidt[17] provide experimental data for the muzzle blast from a 20 mm cannon with counter-recoil force generated by a double-baffle muzzle brake device. Using the muzzle exit conditions of Reference 17, Widhopf, Buell and Schmidt[16] have numerically simulated the near-field muzzle brake flow, by means of a first-order accurate Godunov method. This simulation includes both single- and double-baffle muzzle brake configurations, with and without the inclusion of a projectile. We have chosen the 20 mm cannon (without projectile), single-baffle brake configuration as a computational test for the second-order TVD scheme described herein. For computational economy, the streamwise brake thickness is narrowed, but this should not drastically alter results on the inner surface of the baffle.

From Reference 17, the barrel thickness is 1 D, where $D = 20$ mm is the muzzle diameter. The brake is located 1 D in front of the muzzle exit, with a 1·2 D hole for projectile passage (see Figure 1, where in plotting radial-co-ordinate measurements have been compressed by a factor of 0·6). For subsonic exit flow of the propellant gas immediately behind the projectile, an expansion wave propagating back up the barrel accelerates the propellant gases to the sonic exit condition

$$U^* = a^* = 691 \text{ m/s}, \qquad \gamma = 1{\cdot}25,$$
$$P^*/P_\infty = 111.$$

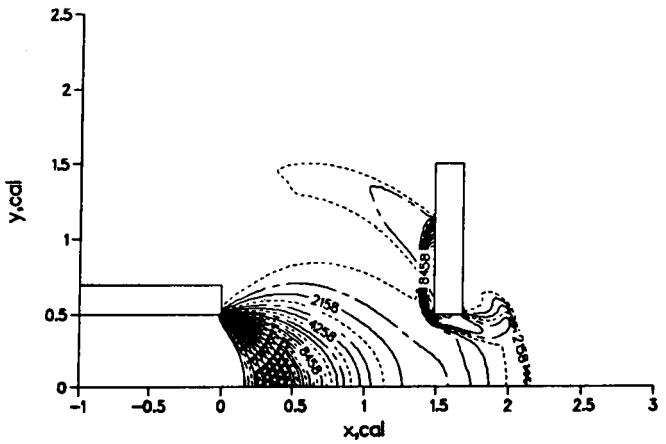

Figure 1. Pressure contours (kPa) for 105 mm Howitzer at 100 μs (67 steps)

Here, a^* is the local speed of sound, and P_∞ is the exterior (atmospheric) pressure level.

Figures 1 and 2 show Mach contour plots at various stages in the evolution of a blast wave from a 105 mm Howitzer test case. In Figure 2, traces of the shock wave impacting on the baffle are clearly visible. Figures 3–5 show the baffle overpressure history at various radial locations on the inner surface of the baffle, for the Gion–Schmidt test case. Table I shows comparison of TVD numerical results against Gion–Schmidt measurements of peak and steady overpressures on the inner surface of the baffle.

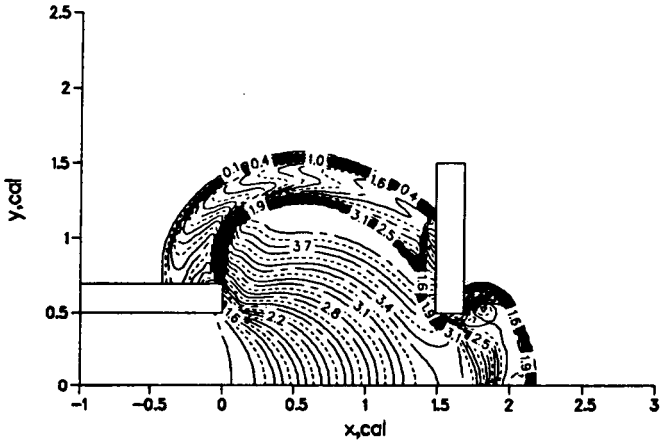

Figure 2. Mach contours for 105 mm Howitzer at 100 μs (67 steps)

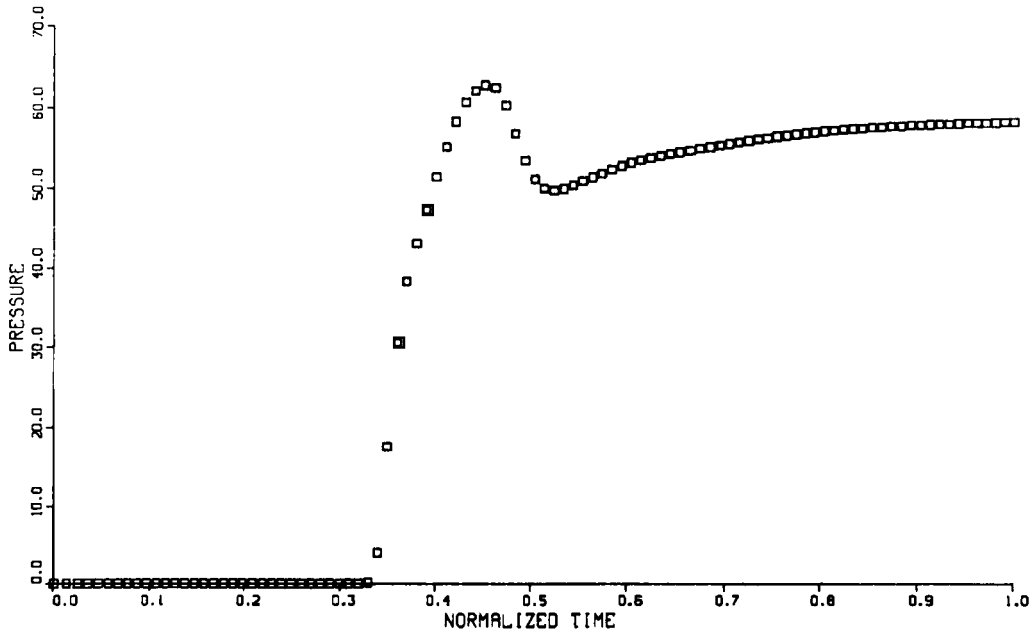

Figure 3. Baffle overpressure history: $R/D = 0{\cdot}5$; $x/D = 1$; time $= 4{\cdot}0181870 \times 10^{-5}$

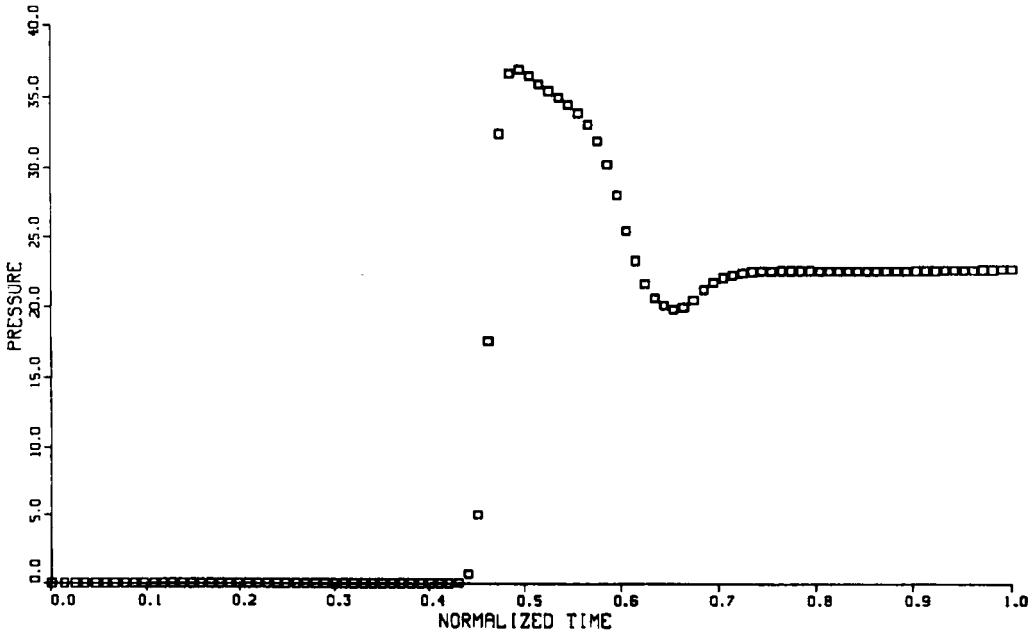

Figure 4. Baffle overpressure history: $R/D = 1{\cdot}0$; $x/D = 1$; time $= 4{\cdot}0181870 \times 10^{-5}$

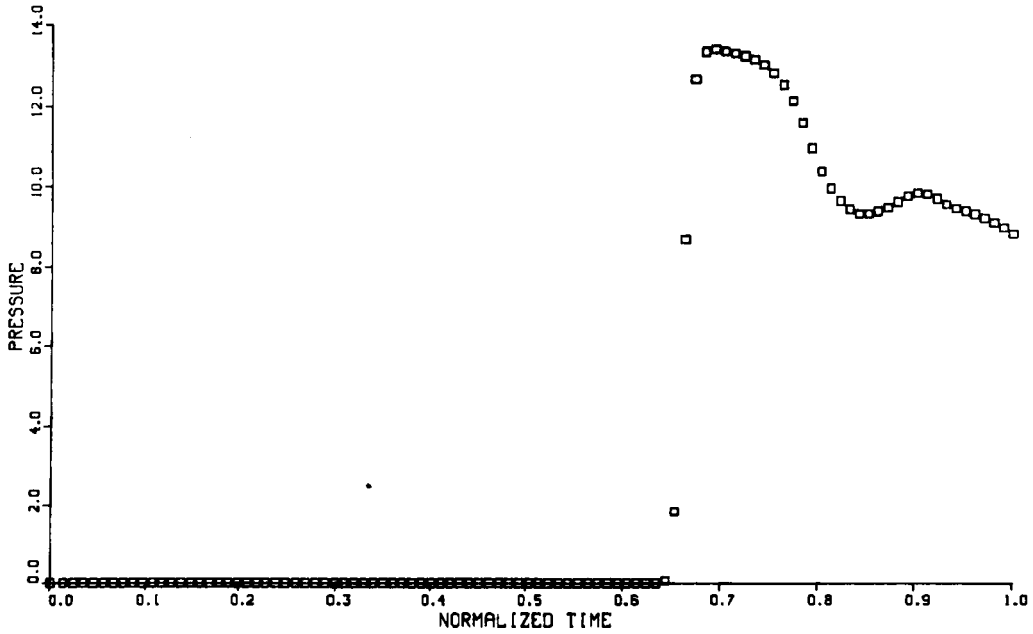

Figure 5. Baffle overpressure history: $R/D = 1{\cdot}5$; $x/D = 1$; time $= 4{\cdot}0181870 \times 10^{-5}$

Table I*. Overpressure ($\bar{p} = (P - P_\infty)/P_\infty$) at $x/D = 1$

$y = R/D$	Peak overpressure		Steady overpressure	
	Gion–Schmidt Figure 5(b)	TVD	Gion–Schmidt Figure 7	TVD
0·5	52†	62	—	—
1·0	31	37	21·0	22·5
1·5	10	13	5·0	$\simeq 6$‡

* The Gion–Schmidt configuration includes the projectile and a double-baffle brake: the TVD configuration is projectile-less with a single-baffle, thinner brake.
† extrapolation; $P_1 = 2P_2 - P_3$
‡ Estimated from Figure 5; clearly well under 8.

Table I indicates TVD peak overpressure calculations roughly twenty per cent in excess of corresponding experimental results. To a lesser degree, this excess is also characteristic of the Godunov[16] calculations, which include the projectile. As results for steady overpressures, achieved after passage of the projectile, are very nearly in agreement, it is expected that adding the projectile simulation to the TVD code should bring closer agreement in the peak overpressure results.

BOUNDARY CONDITION VALIDATION

When a blast wave is impinging upon a muzzle brake device, from the physical standpoint the boundary condition treatment for shockless flow at the wall should differ from the treatment required when an impinging shock wave has traversed the last grid point next to the wall. However, in a typical shock-capturing calculation, no cognizance is taken of the actual shock position. Thus, owing to the absence of knowledge concerning when a shock wave will arrive, the wall boundary condition treatment must be robust enough to be effective in both instances.

For present efforts, the boundary condition treatment of Widhopf and Buell[16] has been employed. From a knowledge of one flow variable (zero normal velocity) at the wall, the Rankine–Huguniot relations may be used to solve for wall pressure (and density). This allows wall flux to be evaluated, assuming that the wall is normal to the grid-line on which Harten's scheme is being applied. (When the wall meets the grid-line on a slant, the tangential velocity must be extrapolated). When the flow in the vicinity of the wall is directed away from the wall, the theory of the eisentropic expansion wave is employed.

With exception of the pressure extrapolation given by Yee, Warming, and Harten,[14] we have studied numerically the effectiveness of the boundary conditions discussed in the preceding section, for the case of one-dimensional flow and a normal shock wave reflecting from a plane wall. The shock is generated by the bursting of a partition separating compartments of a quiescent flow, with diaphragm pressure and density ratio P_2/P_1 and ρ_2/ρ_1. The propagating shock wave has pressure ratio P_3/P_1 if $P_2 > P_1$. Using the results of Landau,[18] the pressure ratio P_4/P_3 for the reflected shock wave can be calculated.

The numerical study indicated the following: for a weak shock, with $P_2/P_1 = 10$, and sufficient mesh, the proper reflection coefficient P_4/P_3 could be accurately approximated, using each boundary treatment studied. Figures 6 and 7 show typical results, for a Widhopf–Buell boundary condition and the first-order accurate Godunov method, as opposed to the same boundary treatment and Harten's second-order method. Results from pure wall reflection and Harten's scheme were essentially the same.

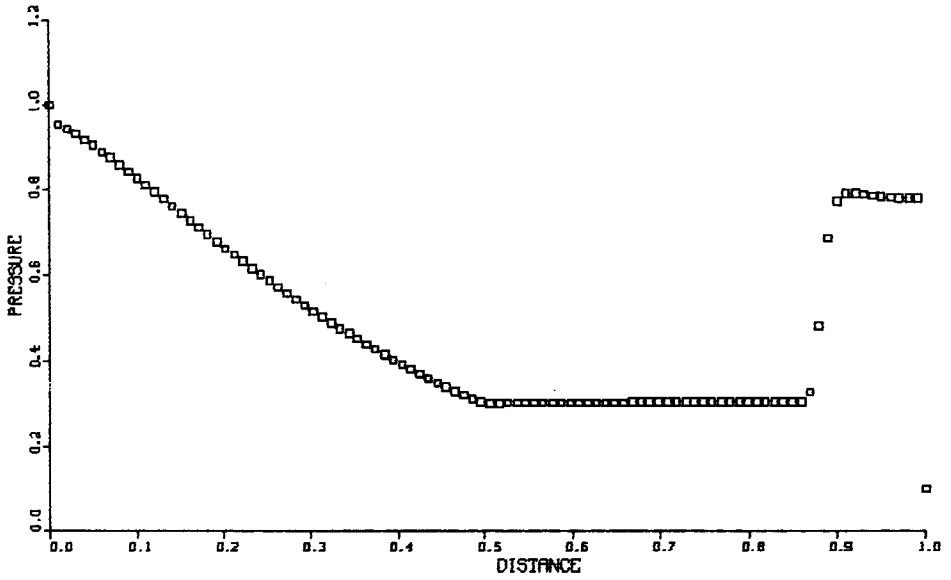

Figure 6. Normal shock reflection; Godunov method: streamwise pressure; time = $1{\cdot}9749430 \times 10^{-1}$

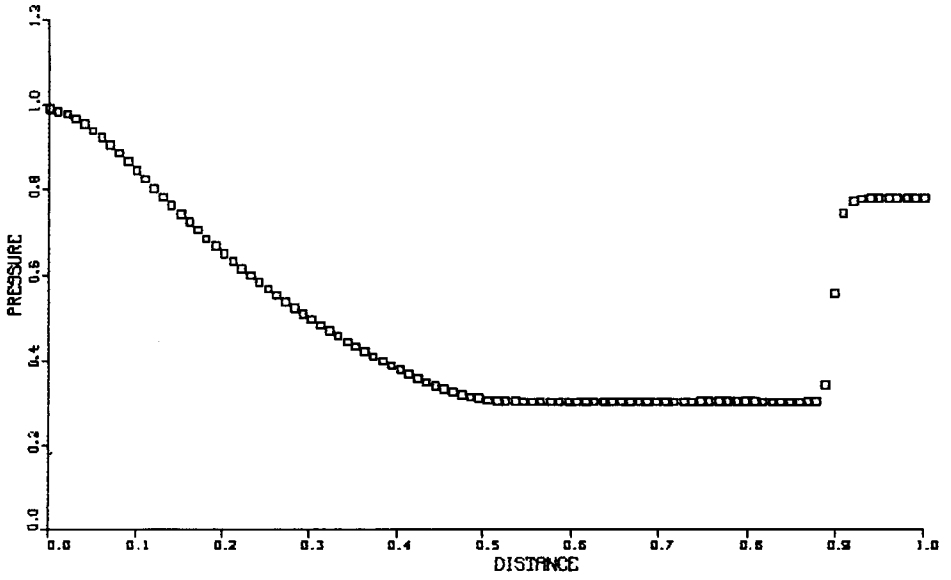

Figure 7. Normal shock reflection; Harten's method: streamwise pressure; time = $1{\cdot}9662630 \times 10^{-1}$

SLANTED BAFFLE NUMERICAL RESULTS

In its original conception, Harten's method[5] requires uniformly spaced grid-points; however, in more recent work[10] it has been applied in curvilinear co-ordinate systems by means of mappings from the physical plane to a uniformly discretized computational plane. An alternative approach in the presence of irregular geometry is the zonal method of Mohan Rai,[19] where uniform grids on different zones are merged at a common boundary by function interpolation. In the present work

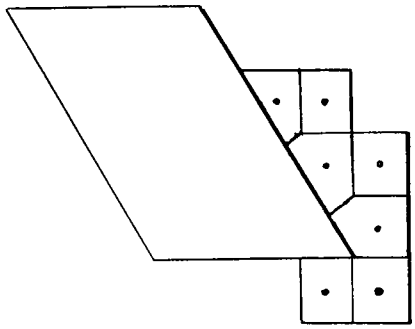

Figure 8. Typical grid merging at a boundary

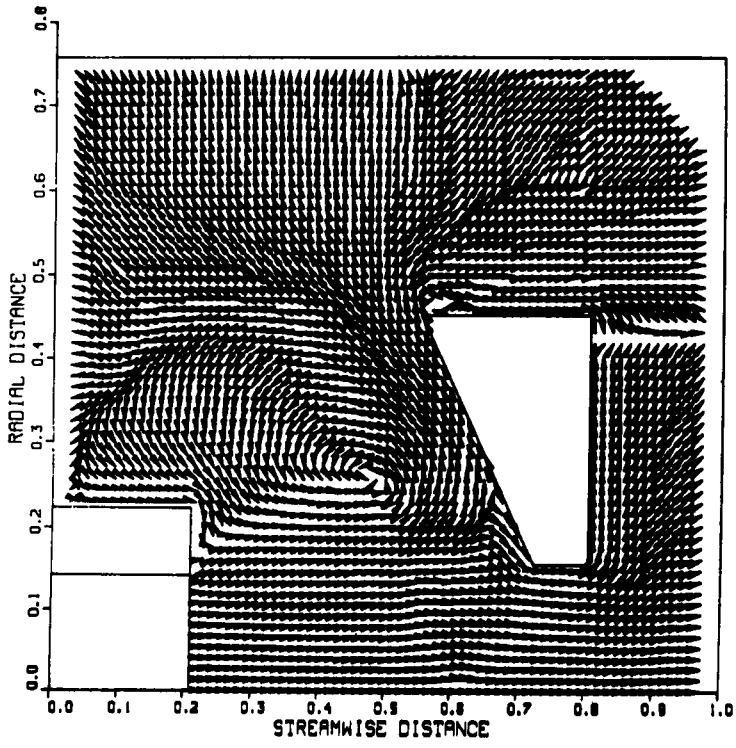

Figure 9. Blast wave progression for slanted baffle: time = $1{\cdot}6723490 \times 10^{-4}$

the complexity of mapping or zonal merging has been avoided through employing a hybrid computational method. Here, an irregular boundary grid is merged with a uniform interior grid, and the Godunov method[1] is used to process irregular cells. Figure 8 shows a typical conception of the merging of regular and irregular cells.

Figure 9 shows velocity vector plots for a typical calculation of the flow from a 30 mm cannon with a single-baffle muzzle brake. The flow is initiated under the assumption of a shock tube driver. At time $t = 0$ a shock with strength

$$p = 3{\cdot}42 \times 10^5\ \mathrm{N/m^2}, \quad \gamma = 1{\cdot}4,$$

is emerging from the barrel into a quiescent flow at atmospheric temperature and pressure. It is assumed that the time interval of interest is sufficiently short that during the course of calculation the driving contact surface does not reach the exit plane, which assumption can be used to initialize the flow interior to the barrel.

Here the muzzle diameter is $D = 30$ mm; the lower edge of the baffle is $1{\cdot}8\ D$ from the exit plane and $0{\cdot}55\ D$ above the line of symmetry. The baffle is inclined thirty degrees from the vertical; it has thickness $0{\cdot}32\ D$, and the top is $1{\cdot}95\ D$ above the axis of symmetry. Owing to the need for computational economy in testing the code, the grid is coarse, and the streamwise limits of the computational plane not sufficiently far removed so as to be certain they will have no effect on the numerical results.

CONCLUSIONS

An algorithm for muzzle blast calculation by numerical means, which employes Harten's second-order shock capturing technique, has been developed. This method can be applied to flows in either Cartesian or axisymmetric co-ordinate systems. Consistency of the operator splittings necessary to apply the method appears validated by the numerical results. It is considered a consistent splitting, and has been proved to be second-order accurate.[9] The method has been applied to numerical simulation of blast wave progression in the presence of vertical and slanted muzzle-brake devices.

REFERENCES

1. S. K. Godunov, *Math. Sb.*, **47,** 271 (1959).
2. G. A. Sod, 'A survey of several finite difference methods for systems of hyperbolic conservation laws', *J. Comp. Phys.*, **27,** 1–31 (1978).
3. B. Van Leer, 'Towards the ultimate conservative difference scheme, V. A second order sequel to Godunov's method', *J. Comp. Phys.*, **32,** 101–136 (1979).
4. P. Colella and P. R. Woodward, 'The piecewise parabolic method (PPM) for gas dynamical simulations', *LBL Report No. 14661*, July 1982.
5. A. Harten, 'High resolution schemes for hyperbolic conservation laws', *J. Comp. Phys.*, **49**, 357–393 (1983).
6. P. L. Roe, 'The use of the Riemann problem in finite difference schemes', *Proceedings, Seventh International Conference on Numerical Methods in Fluid Dynamics*, NASA, Ames Research Center, June 1980; Springer-Verlag, Berlin, 1981, p. 354.
7. S. R. Chakravarthy and S. Osher, 'Numerical experiments with the Osher upwind scheme for the Euler equations', *AIAA Journal*, **21** (9), 1241 (1983).
8. G. Strang, 'On the construction and comparison of difference schemes', *SIAM J. Num. Anal.*, **5** (3), 506–517 (1968).
9. C. H. Cooke, 'On operator splitting for time varying boundary value problems', *Comp. Physics*, **67,** (2), 472–478 (1986).
10. H. C. Yee and P. Kutler, 'Application of second-order accurate, total variation diminishing (TVD) schemes to the Euler equations in general geometries', *NASA TM-85845*, Ames Research Center, Moffet Field, California, August 1983.
11. G. Carofano, 'Secondary waves from nozzle blast', *U.S. ARDC Technical Report No. ARLCB-TR-84*, Benet Weapons Laboratory, Watervliet, N.Y., 1984.
12. R. F. Warming, R. Beam and B. J. Hyett, 'Diagonalization and simultaneous symmetrization of the gas dynamic matrices', *Math. Comp.* **29** (132), 1037–1045 (1975).
13. P. L. Roe, 'Approximate Riemann solvers, parameter vectors, and difference schemes', *J. Comp. Phys.*, **43,** 357–372 (1981).
14. H. C. Yee, R. F. Warming and A. Harten, 'Implicit total variation diminishing (TVD) schemes for steady state calculations', *J. Comp. Phys.*, **49,** 377–393 (1983); also, *NASA TM-84342.*
15. G. C. Carofano, 'Blast computation using Harten's TVD scheme, *U.S. Army Internal Memorandum*, Watervliet Arsenal, 1984.
16. G. F. Widhopf, J. C. Buell and E. M. Schmidt, 'Time dependent near-field muzzle brake flow simulations', *AIAA-82-0973, AIAA/ASME 3rd Joint Thermophysics, Fluids, Plasma and Heat Transfer Conference*, St. Louis, Missouri, 7–11 June 1982.
17. J. Edmond Gion and M. Edward Schmidt, 'Measurements on a circular plate immersed in muzzle flow', *BRL-MR-2762*, Armament Research and Development Command, Ballistic Research Laboratory, Aberdeen Proving Ground, Maryland, June 1977.

18. L. D. Landau and E. M. Lifschitz, *Fluid Mechanics*, Pergamon Press, London, 1959.
19. M. M. Rai, 'A conservative treatment of zonal boundaries for Euler equation calculations', *AIAA-84-0164, AIAA Twenty-second Aerospace Sciences Meeting*, Reno, Nevada, 9–12 January 1984.
20. C. H. Cooke, 'On operator splitting of the Euler equations consistent with Harten's TVD scheme', *Numerical Methods For Partial Differential Equations*, **1**, 315–327 (1985).